Solution-Processed Squaraine Bulk Heterojunction Photovoltaic Cells

Guodan Wei,[†] Siyi Wang,[‡] Kyle Renshaw,[§] Mark E. Thompson,[‡] and Stephen R. Forrest[†,§,⊥,*]

[†]Department of Materials Science and Engineering, University of Michigan, Ann Arbor, Michigan 48109, [‡]Department of Chemistry, University of Southern California, Los Angeles, California 90089, [§]Department of Applied Physics, University of Michigan, Ann Arbor, Michigan 48109, and [⊥]Department of Electrical Engineering and Computer Science, University of Michigan, Ann Arbor, Michigan 48109

ABSTRACT The donor, 2,4-bis[4-(*N*,*N*-diisobutylamino)-2,6-dihydroxyphenyl] squaraine (SQ) is used with the acceptor, [6,6]-phenyl C_{70} butyric acid methyl ester ($PC_{70}BM$) to result in efficient, solution-processed, small-molecule bulk heterojunction photovoltaic cells. The distribution of the donor nanoparticles in the acceptor matrix as a function of relative concentrations results in a trade-off between exciton dissociation and hole mobility (and hence, cell series resistance). A bulk heterojunction solar cell consisting of an active region with a component ratio of SQ to $PC_{70}BM$ of 1:6 has a power conversion efficiency of 2.7 ± 0.1% with a 8.85 ± 0.22 mA/cm^2 short-circuit current density and an open-circuit voltage of 0.89 ± 0.01 V obtained under simulated 1 sun (100 mW/cm^2) air mass 1.5 global (AM1.5 G) solar illumination. This is a decrease from 3.3 ± 0.3% at 0.2 sun intensity, and is less than that of a control planar heterojunction SQ/C_{60} cell with 4.1 ± 0.2% at 1 sun, suggesting that the nanoparticle morphology introduces internal resistance into the solution-based thin film. The nanomorphology and hole mobility in the films is strongly dependent on the SQ-to-$PC_{70}BM$ ratio, increasing by greater than 2 orders of magnitude as the ratio increases from 28% to 100% SQ.

KEYWORDS: solar cell · photovoltaic · bulk heterojunction · small molecule · solution processing

Bulk-heterojunction (BHJ) solar cells based on interpenetrating blends of electron- and hole-transporting materials offer promise for low-cost, sustainable, electricity production.[1−3] Efficient charge generation throughout the active blends, ultrafast charge transfer at the donor/acceptor interface, and efficient charge transport are essential for high performance photovoltaic applications.[4] Because of the potentially low-cost of fabrication, solution processing has been widely explored to demonstrate polymeric bulk solar cells with high power efficiencies,[5−7] although the dependence of performance on polymer materials such as regioregularity, polydispersity, and stability[8] have not been fully addressed.

In contrast, small molecules are intrinsically monodisperse and simple to synthesize and purify. In general, the concept of the bulk heterojunction has been demonstrated in small-molecular weight organic solar cells with active layers codeposited by vacuum thermal evaporation[9] or organic vapor phase deposition.[10] There are also examples of small molecules that have been used as solution processable donor materials in BHJ architectures.[11−13] Unfortunately, the strong intermolecular forces between conjugated small molecules can result in the nucleation of molecular crystals in solution, generating incomplete film coverage with high surface roughness in such BHJs. To obtain improved performance, efforts have focused on the design and synthesis of soluable donors with high charge carrier mobility and absorption in the visible and new-infrared spectral regions, in combination with a high interfacial gap energy at the donor−acceptor interface.[8] Among these, 2,4-bis[4-(*N*,*N*-diisobutylamino)-2,6-dihydroxyphenyl] squaraine (SQ) dyes with hydroxyl groups at the 2,6-positions of the two phenyl rings[14] have been identified as donors that absorb at wavelengths $\lambda > 650$ nm which, when combined with a C_{60} acceptor layer, have a larger open circuit voltage (V_{oc}) than that of the commonly used copper phthalocyanine (CuPc)/C_{60} cell.[15] This particular squaraine is attractive since the addition of the four hydroxyl groups gives the compound added stability over alternative formulations and it can be vacuum sublimed without decomposition.

In this paper, we show that the combination of the optical, electrical, and chemical properties of SQ blended in solution with [6,6]-phenyl C_{70} butyric acid methyl ester ($PC_{70}BM$) in a 1:6 mixture results in cells with power conversion efficiency $\eta_p = 2.7 \pm 0.1\%$, short-circuit current density $J_{sc} = 8.85 \pm 0.22$ mA/cm^2, and $V_{oc} = 0.89 \pm 0.01$ V at 1 sun intensity, AM1.5G simulated solar emission, and a peak external quantum efficiency EQE = 48% at a wavelength of $\lambda = 385$ nm. Its peak $\eta_p = 3.3 \pm 0.3\%$ at 0.2

*Address correspondence to stevefor@umich.edu.

Received for review December 20, 2009 and accepted March 18, 2010.

Published online April 1, 2010.
10.1021/nn100195j

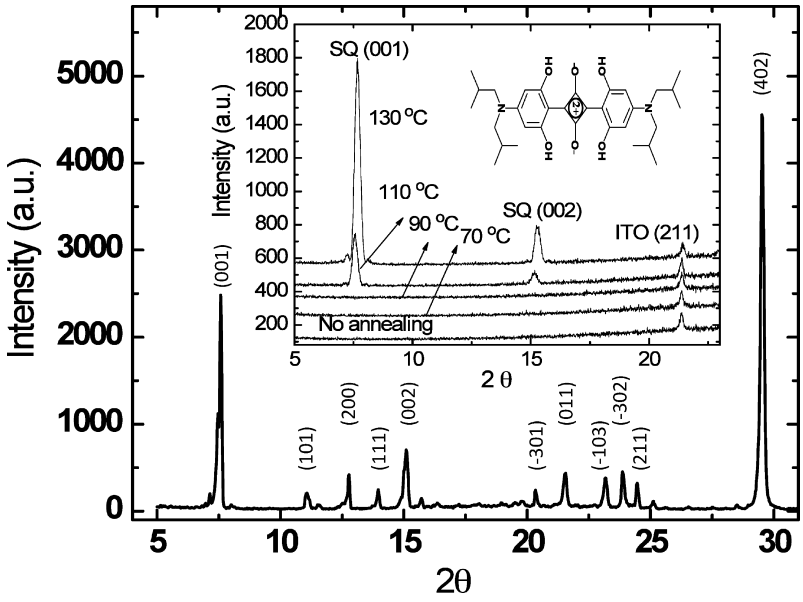

Figure 1. X-ray-diffraction (XRD) patterns of squaraine (SQ) bulk powder materials. Inset: SQ thin film spin-coated from dichloromethane solvent on indium tin oxide (ITO) coated glass substrates. The diffraction peaks are indexed using Winplotr and FullProf[17,18] software routines. XRD spectra indicate that the neat SQ film annealed at 110 and 130 °C has the same crystal structure as the powder, with the (001) and (002) crystal axes normal to the substrate plane. No peaks are found for any of the SQ:$PC_{70}BM$ blended films, indicating that they are amorphous. Also shown in the inset is the molecular structural formula of SQ.

sun is compared with a control, planar heterojunction SQ/C_{60} cell with an efficiency of 4.1 ± 0.2% at 1 sun (correcting for solar mismatch). We show that the morphology of the SQ:$PC_{70}BM$ composites affects the hole transport mobility, resulting in an unbalanced electron and hole transport and relatively low fill factor (FF). The higher efficiency of the control SQ/C_{60} device is due to the nanocrystalline interdigitated bilayer morphology, resulting in high hole mobility and hence efficient charge collection efficiency.

RESULTS

The molecular structural formula (inset of Figure 1) for the SQ contains two phenyl rings with four hydroxyl groups that result in its solubility.[14] Its thermal properties have been previously reported,[16] with a melting point of 294 °C and a deposition temperature of 299 °C. The SQ powder characterized by XRD (Figure 1) indicates a monoclinic unit cell [space group *P2/m* with $a = 14.95$, $b = 9.35$, $c = 11.50$ Å, $\beta = 98.20°$].[17,18] Thin films annealed at 110 and 130 °C for 10 min exhibit (001) and (002) peaks at $2\theta = 7.58°$ and $2\theta = 15.29°$ (inset, Figure 1) corresponding to an intermolecular spacing of $d_{002} = 5.75$ Å. There are no peaks for SQ, $PC_{70}BM$, and SQ:$PC_{70}BM$ blends with five different ratios of 3:1, 1:1, 1:2, 1:3, and 1:6 annealed at 70 °C, indicating amorphous films.

The absorption spectra of pure SQ and blends of SQ:$PC_{70}BM$ films annealed at 70 °C on quartz substrates are shown in Figure 2. The SQ absorption extends to wavelengths of $\lambda = 750$ nm with a peak at $\lambda = 680$ nm. When mixed with $PC_{70}BM$ with absorptions centered at $\lambda = 375$ and $\lambda = 465$ nm, the resulting film has coverage across the visible spectrum. As the fraction of $PC_{70}BM$ increases, the SQ absorption peak is suppressed, with a concomitant increase in absorption from $\lambda = 300$ to $\lambda = 500$ nm, characteristic of $PC_{70}BM$.

In Figure 3, inset, we plot the *J*−*V* characterisitcs of a hole-only device with a 1:1 SQ:$PC_{70}BM$ blend, with the top cathode biased positive with respect to the anode. The data follow $J \propto V^2$ and hence are fit to a trap-free space charge limited model[19] to extract the zero-field hole mobility (μ_0) as shown. Here, μ_0 decreases from 1×10^{-5} to 1.2×10^{-7} $cm^2/(V\ s)$ when the molecular weight percentage of SQ decreases from 100% (pure SQ thin films) to 28%. A minimum of 4×10^{-8} $cm^2/(V\ s)$ is obtained for a 1:3 mixture (corresponding to 42 wt % SQ in $PC_{70}BM$). With the exception of the 100% SQ control device, the lowest mobility is obtained for the roughest films. Indeed, in the mixed films, we show later that the hole mobility along discontinuous conduction pathways limits cell performance in contrast to electron mobility in $PC_{70}BM$.

The EQE (Figure 4) and *J*−*V* (Figure 5) characteristics of the blended and control solar cells are summarized in Table 1. The addition of $PC_{70}BM$ broadens the spectral response of the cells into the wavelength range from $\lambda = 450$ to 600 nm. The 3:1 and 1:1 blend film devices show EQE < 22% at the absorption peak of SQ, in-

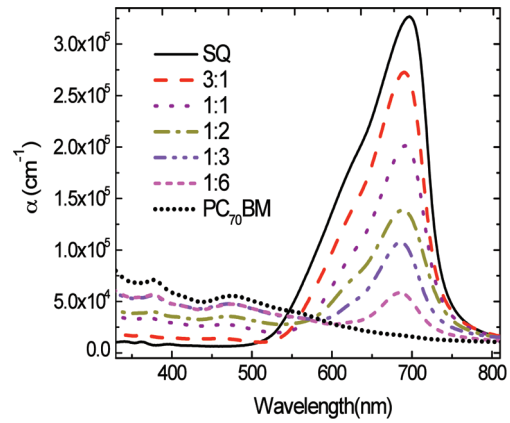

Figure 2. The absorption coefficient (α) of pure squaraine, $PC_{70}BM$, and blends of both materials on quartz substrate with SQ:$PC_{70}BM$ ratios of 3:1, 1:1, 1:2, 1:3, and 1:6.

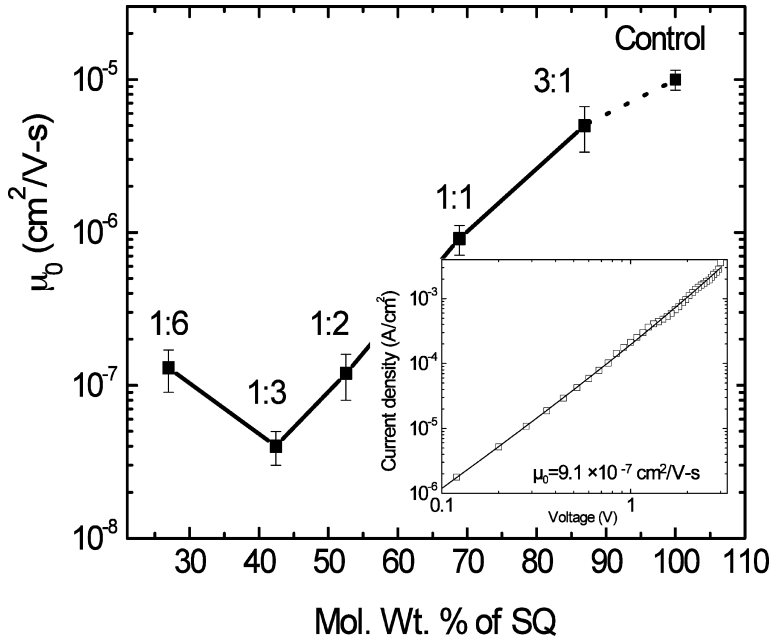

Figure 3. The zero-field hole hole mobility (μ_0) *versus* molecular weight ratio between squaraine and $PC_{70}BM$. Inset: Typical current density *vs* voltage characteristic of samples used for mobility measurement. A fit to the data (straight line) gives $\mu_0 = 9.1 \times 10^{-7}$ cm^2/(V s) for a SQ:$PC_{70}BM$ 1:1 blend.

creasing to 48% at $\lambda = 385$ nm (due to $PC_{70}BM$) for a 1:6 mixture. Comparison with the absorption characteristics in Figure 2 indicate that the relative balance between the EQE due to SQ and $PC_{70}BM$ absorption in the mixed cells suggests that charge collection, and not exciton dissociation, governs cell performance.

In Figure 5, we show the $J-V$ characteristics at very low (Figure 5a) and at 1 sun intensity (Figure 5b) AM1.5G illumination. At the higher intensities, we find

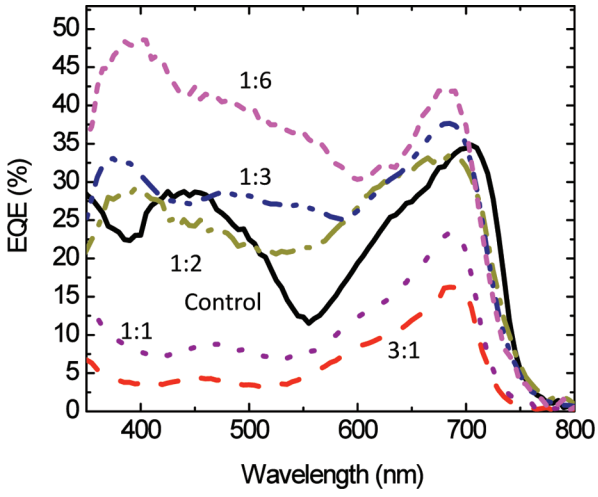

Figure 4. The effect of SQ:$PC_{70}BM$ blend ratios on the external quantum efficiency (EQE) for the five bulk cells with a device structure of ITO/MoO_3(80 Å)/SQ:$PC_{70}BM$(*x* Å)/Al(1000 Å), and the EQE of the SQ/C_{60} planar control cell with a device structure of ITO/MoO_3(80 Å)/SQ(62 Å)/C_{60}(400 Å)/bathocuproine (BCP)(100 Å)/Al(1000 Å). Here, *x* = 320, 400, 720, 730, and 760 Å for the five blend cells with compositions 3:1, 1:1, 1:2, 1:3 and 1:6, respectively.

that V_{oc} ranges from 0.75 to 0.90 V as shown in Figure 6a, with the higher values corresponding to cells with a low FF. Hence, the largest open circuit voltages are due, in part to the higher resistance of the cells. Nevertheless, these V_{oc} are consistently higher than previously reported 0.62 V for the SQ:$PC_{60}BM$ bulk cells,[11] as a result of the lower saturation dark current, J_0, of our MoO_3 based cells (see Table 1).

The fill factors and power conversion efficiencies of the solution-processed solar cells are shown in Figures 6b and 7, respectively. The incorporation of a MoO_3 buffer layer leads to a reduction in dark current arising from electron leakage to the anode[20] and hence a concomitant increase in V_{oc}. The SQ/C_{60} control cells have the highest fill factor of FF = 0.54 ± 0.02 at 1 sun intensity, compared to FF = 0.26 to 0.35 for the SQ:$PC_{70}BM$ cells (Table 1). Because of the low fill factor, the power conversion efficiency of the 1:6 SQ:$PC_{70}BM$ cell drops from 3.0 ± 0.3% with FF = 0.38 ± 0.01 at 0.2 sun (20 mW/cm^2) AM1.5G illumination, to $\eta_p = 2.7 \pm 0.1\%$ with FF = 0.35 ± 0.01 at 1 sun. This is comparable to the SQ/C_{70} planar cell, with $\eta_p = 2.7 \pm 0.1\%$, $V_{oc} = 0.72 \pm 0.01$ V, and FF = 0.45 ± 0.02 under similar illumination conditions. It is notable that the performance of both the 1:6 SQ:$PC_{70}BM$ and SQ:$PC_{60}BM$ cells are qualitatively similar, as apparent in Table 1. The somewhat reduced V_{oc} of the latter cell is due to the comparatively large $J_0 = 1.6 \times 10^{-5}$ mA/cm^2, *vs* 6.2×10^{-7} mA/cm^2 for the $PC_{70}BM$-based cell.

The highest efficiencies achieved are with the 1:2 blended films at low illumination intensity and the planar SQ/C_{60} control device at 1 sun intensity, both peaking at 4.1 ± 0.2%. Note that introducing a bathocuproine blocking layer between the cathode and C_{60}, as is typical of high performance planar junction cells,[10] reduces the efficiency to 2.7% in the control cell. As in the case of the 1:6 blended cell, the 1:2 cell efficiency falls off sharply with light intensity, along with a concomitant decrease in FF. In contrast, the unblended, planar control with its relatively high and intensity-independent FF shows only a weak efficiency dependence as intensity is varied from 0.01 to 2 suns.

DISCUSSION

Examination of the AFM images of the pure SQ, pure $PC_{70}BM$ and their blended films as deposited

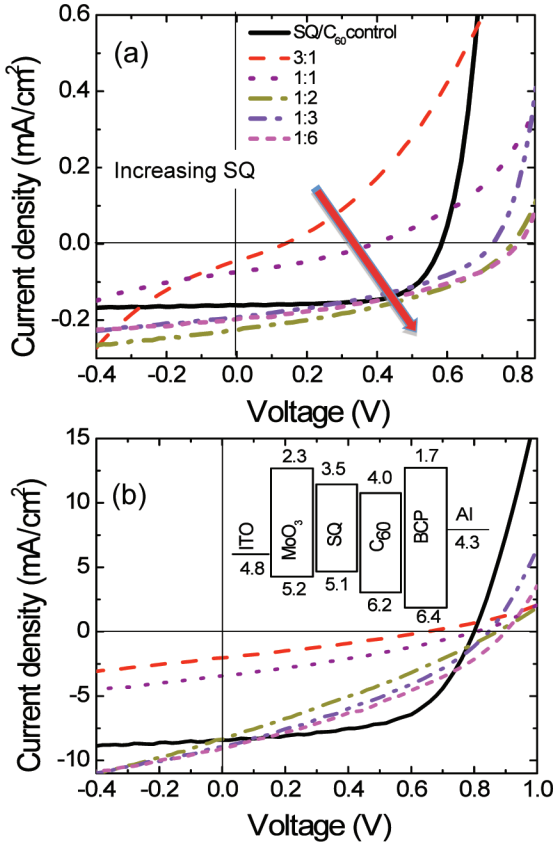

Figure 5. Current density−voltage ($J-V$) characteristics illuminated at (a) 0.02 sun; (b) 1 sun for the SQ:$PC_{70}BM$ blended bulk cells, and the SQ/C_{60} planar control cell. Inset shows the energy level diagram of the SQ:C_{60} control cell.

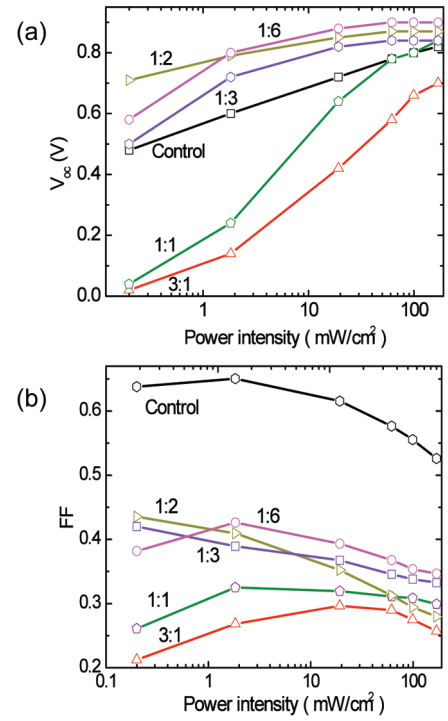

Figure 6. (a) Open circuit voltage (V_{oc}), and (b) fill factor (FF) as functions of AM1.5G spectral illumination power (corrected for solar spectral mismatch) of the five blended SQ:$PC_{70}BM$ cells and the squaraine/C_{60} planar control cell.

on 80 Å thick MoO_3 buffer layers shown in Figure 8 suggest that film nanomorphology largely controls the cell performance and the hole mobility (Figure 3). While the pure, nanocrystalline SQ film in Figure 8c has a root-mean-square (rms) roughness of 1.7 ± 0.02 nm, those containing neat $PC_{70}BM$ are very smooth with a rms roughness of only 0.55 ± 0.04 nm (Figure 8a). The active layer roughness of five blends for the ratios of 3:1, 1:1, 1:2, 1:3. and 1:6 are plotted in Figure 8d, and indicate a surface sufficiently smooth to fabricate devices with films free of pinholes and other macroscopic defects. At the highest SQ concentrations, the decreased roughness of <0.8 nm indicates amorphous SQ clusters that are likely separated by intervening $PC_{70}BM$. The separate domains of SQ in a matrix of $PC_{70}BM$ are apparent in Figure 8b for a 1:3 SQ:$PC_{70}BM$ blend. The tendency of SQ to aggregate leads to a surface with a roughness of 1.6 ± 0.1 nm. Note that at this concentration, the hole mobility has a minimum value of 4×10^{-8} $cm^2/(V\ s)$, indicating a nonuniform distribution of SQ domains throughout the blend.

The highest efficiencies are achieved for the planar SQ/C_{60} devices, where the SQ is both rough (Figure 8) and crystalline (Figure 1, inset). In this case, the rms roughness of 1.7 nm is characteristic of the crystallite size and is on the order of an exciton diffusion length in such materials.[21] Hence, the rough interface between SQ and C_{60} forms a nanocrystalline interdigitated bilayer or BHJ similar to that previously demonstrated between CuPc and C_{60} grown by organic vapor phase deposition.[10] Note that the considerably lower efficiency obtained for the control SQ/C_{70} cell than for the

TABLE 1. Summary of Solar Cell Characteristics of Different SQ:$PC_{70}BM$ Blend Ratios and a SQ/C_{60} Planar Control Cell

SQ:$PC_{70}BM$ ratio	V_{oc} (V)	J_{SC} (mA/cm^2)	FF	J_0 (mA/cm^2)	η_p (%) at P_0 = 1 sun	η_p (%) (max)	P_0 at max η_p (mW/cm^2)
3:1	0.68(±0.03)	1.79(±0.19)	0.26(±0.01)	2.8×10^{-2}	0.32(±0.01)	0.32(±0.01)	100
1:1	0.81(±0.01)	3.61(±0.03)	0.31(±0.01)	1.1×10^{-2}	0.90(±0.01)	0.90(±0.01)	100
1:2	0.87(±0.01)	8.33(±0.50)	0.29(±0.01)	3.7×10^{-7}	2.1(±0.1)	4.1(±0.2)	2
1:3	0.84(±0.01)	8.83(±0.34)	0.33(±0.01)	8.7×10^{-6}	2.4(±0.1)	3.0(±0.1)	2
1:6	0.89(±0.01)	8.85(±0.22)	0.35(±0.01)	6.2×10^{-7}	2.7(±0.1)	3.3(±0.1)	20
1:6/BCP	0.84(±0.01)	9.33(±0.12)	0.36(±0.01)	2.7×10^{-7}	2.9(±0.2)	3.8(±0.2)	0.2
SQ:$PC_{60}BM$1:6	0.78(±0.01)	9.17(±0.25)	0.42(±0.01)	1.6×10^{-5}	3.0(±0.1)	3.6(±0.1)	2
SQ/C_{60}	0.79(±0.01)	8.90(±0.25)	0.54(±0.02)	1.2×10^{-6}	3.8(±0.2)	4.1(±0.2)	100
SQ/C_{70}	0.72(±0.01)	8.29(±0.25)	0.45(±0.02)	1.1×10^{-5}	2.7(±0.2)	3.1(±0.2)	20

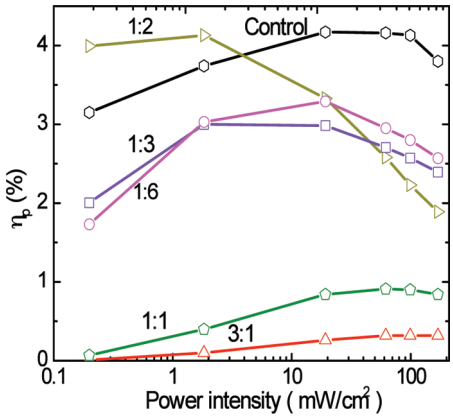

Figure 7. Power conversion efficiency (η_p) as a function of AM1.5G spectral illumination power (corrected for solar spectral mismatch) of the five blended SQ:$PC_{70}BM$ cells and the squaraine/C_{60} planar control cell. The highest efficiencies are 4.1 ± 0.2% for the control (at 1 sun) and the 1:2 (at 0.02 suns) cells.

SQ/C_{60} (Table 1) device may be due to lower purity of the C_{70}. This is also apparent from its roll off in efficiency and fill factor at high intensities, indicative of high series resistance.

While exciton dissociation in uniform blends with a high SQ content (*e.g.*, 1:1 and 3:1) is expected to be efficient, the EQE of these devices is low, and the resulting solar cells are inefficient, particularly at light intensities of >0.1 sun. Hence, we infer that the donor−acceptor interfaces in these mixtures often lie beyond a diffusion length of the exciton generation sites. We note, however, that the hole mobility for such mixtures is comparatively high. This suggests that SQ forms continuous conducting pathways for holes between anode and cathode. To test this assumption, we measured the parallel resistances of the PV cells by fitting their dark current *versus* voltage characteristics to the modified Shockley Equation:[22]

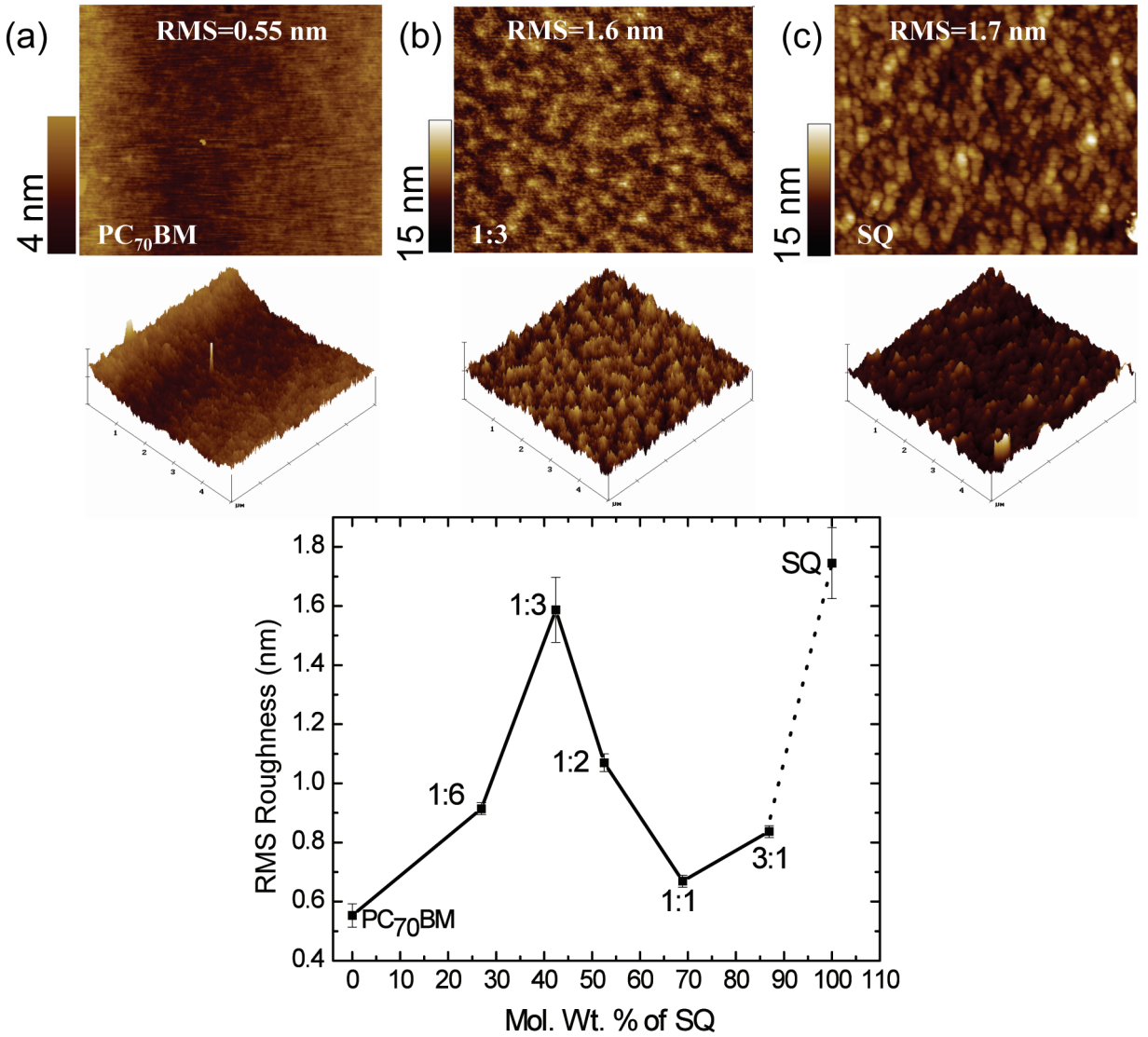

Figure 8. Atomic force microscope topographic and 3D images of (a) pure $PC_{70}BM$, (b) 1:3 SQ:$PC_{70}BM$, and (c) pure SQ films deposited on indium tin oxide coated glass. The field of view of each film is 5 μm × 5 μm. (d) The root-mean-square (rms) roughness *versus* the molecular weight ratio of squaraine blended into $PC_{70}BM$ taken from AFM data as shown in images a−c.

$$J = J_0\left[\exp\frac{q(V - JR_s)}{nkT} - 1\right] + \frac{V - JR_s}{R_p}$$

where q is the electron charge, n is the ideality factor R_s is the diode specific series resistance, and R_p is its specific parallel (or shunt) resistance. The resulting values for J_0 and R_p are shown in Table 1 and Figure 9, respectively, indicating that the films with large concentrations of SQ have a very low parallel resistance, consistent with the existence of shorts formed by percolating hole transport pathways. These pathways also lead to very high J_0 and hence suppressed V_{oc}. Indeed, from the correlation between the increase in *dark current* and R_p, we can rule out field-dependent dissociation of photogenerated geminate electrons and holes at entangled donor−acceptor interfaces as the source of decreased resistance at high SQ content.

Photoelectron spectroscopy measurements indicate an ionization potential energy (IPE) for SQ of 5.1 eV, compared to 6.2 eV for C_{60} (inset, Figure 5b). Including the energy gap for C_{60} of $E_G(C_{60}) = 2.2$ eV, we obtain an interface gap between SQ and C_{60} of 1.1 eV. (Here, the interface energy gap is equal to $\Delta E_G = \mathrm{IPE}(C_{60}) + E_G(C_{60}) - \mathrm{IPE(SQ)}$.) While this is larger than the measured $V_{oc} = 0.9$ V as shown in Figure 6a for a cell with a 1:6 blend, the value is nevertheless considerably improved compared to that for the archetype CuPc/C_{60} cell, where $\Delta E_G = 1.3$ eV *versus* $V_{oc} = 0.55$ V.[23] The high V_{oc} in the blended cells is due to their relatively large series resistance, which is clearly apparent in Figure 5, which results in a low FF and a flattening of the $J-V$ characteristics near $J = 0$. Nevertheless, the V_{oc} of the low series resistance control is 0.79 eV, indicative of reduced recombination (and hence lower dark current) as compared to a conventional CuPc-based cell.[23−25]

An increase of $PC_{70}BM$ concentration to 1:2, 1:3, and 1:6 increases the formation of electron conducting pathways to the cathode. This also reduces the probability for hole shunts formed by the SQ regions while increasing the interfacial area between donor and acceptor regions in the bulk heterojunction. While the surface roughness is relatively high in these mixtures, the improved bulk heterojunction morphology ultimately results in higher efficiencies, even at high illumination intensities. Note also that there is no significant increase of the EQE photoresponse contributed by the SQ donor (Figure 4) at a wavelength of $\lambda = 685$ nm for these bulk cells. In contrast, there is a doubling in the EQE in the wavelength range from $\lambda = 350$ to 600 nm, due to $PC_{70}BM$ absorption. As noted above, the relative balance in magnitude of EQE from both $PC_{70}BM$ and SQ across the wavelength region from 350 to 750 nm compared to the absorption characteristics of these mixtures in Figure 2 indicates that *carrier conduction* limits the cell response, while the mixtures support very efficient exciton diffusion and dissociation at the high surface area interface between donor and acceptor regions. This observation is supported by the relatively low EQE of the nanocrystalline SQ/C_{60} control cell, especially at short wavelengths where we expect that exciton dissociation, and not charge collection limits cell performance.

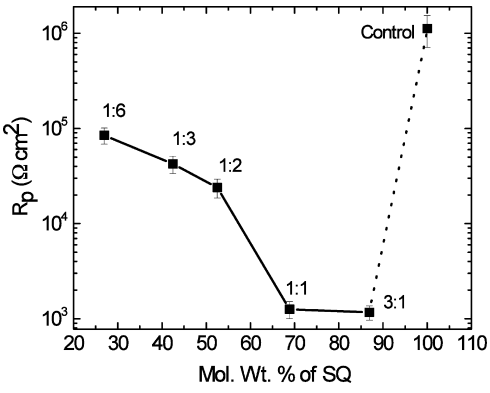

Figure 9. Parallel resistance (R_p) *versus* the molecular weight ratio between squaraine and $PC_{70}BM$ obtained from fitting the current density characteristics using the modified Shockley Equation (see text) of solar cells shown in Figures 4−7. Also shown is the parallel resistance for the SQ/C_{60} control cell.

At SQ:$PC_{70}BM$ mixtures of 1:8 or larger, shorts are formed due to continuous conducting paths of this electron acceptor between anode and cathode. This sets an upper bound to the amount of $PC_{70}BM$ that can be used in the bulk heterojunction before it loses its nanoscale network that can efficiently dissociate excitons. Furthermore, none of the mixtures show a crystalline morphology, as indicated by the XRD patterns for thin film blends shown in Figure 1. This lack of crystallinity is primarily responsible for the relatively low mobilities and hence fill factors and power conversion efficiencies at high illumination intensities in these blended cells, in contrast to the homogeneous, planar SQ/C_{60} control devices.[14]

Indeed, the relatively high FF (0.54 ± 0.02) of the SQ/C_{60} planar control cell results from its high hole mobility and hence high charge collection efficiency.[26] The lack of a continuous interpenetrating network of SQ domains in the blended cells ultimately limits their performance to less than that of the planar junction.[27,28] Therefore, further control of the nanoscale morphology and crystallinity in the SQ:$PC_{70}BM$ composites, possibly achieved by employing a higher annealing temperature, is required. Since the power efficiencies of the 1:2 bulk and planar junctions are similar at low intensities even though the EQE of the latter cell is higher, we suggest that modification of the SQ molecules to form such morphologies may ultimately lead to power conversion efficiencies significantly in excess of 4% at high intensities for these solution-processed junctions.

CONCLUSIONS

Using a combination of XRD, AFM, and measurements of hole mobilities in interpenetrating networks

of SQ and $PC_{70}BM$, we have demonstrated a series of solution-processed, small-molecule SQ:$PC_{70}BM$ solar cells with various donor-to-acceptor constituent ratios. We find that the 1:2 SQ:$PC_{70}BM$ cells have peak efficiencies at low light levels of 4.1 $\pm$ 0.2% (solar spectral mismatch corrected), which is comparable to that of the control, solution+vacuum deposited planar nanocrystalline SQ/C_{60} cells (4.1 $\pm$ 0.2%). However, these latter structures maintain their high efficiency even at intensities exceeding 1 sun, AM1.5G simulated solar intensity.

We have shown that the performance of these cells is largely determined by the nanomorphology of the bulk heterojunctions formed during film deposition and subsequent annealing. The roll off in efficiency (which is due to a roll off in FF) at high intensities in the blends, but not observed in the planar junction control cells, arises from the formation of discontinuous pathways for electron and hole transport. However, the blended films have a more uniform and higher EQE than that of the planar device, suggesting that further control of the nanostructure, possibly using a modified SQ molecule with a higher potential for $\pi-\pi$ stacking into a regular, crystalline structure, can result in increased efficiency at high illumination intensities.

EXPERIMENTAL SECTION

X-ray-diffraction (XRD) patterns of the SQ powder plus the neat SQ, $PC_{70}BM$ (American Dye Source, Inc.) and SQ:$PC_{70}BM$ (in weight concentrations of 3:1, 1:1, 1:2, 1:3, and 1:6) thin films spin-coated on indium tin oxide (ITO) substrates at a rate of 3000 rpm (revolutions per minute) were obtained using a Rigaku diffractometer in the $\theta-2\theta$ geometry using a 40 kV Cu Kα radiation source. The neat SQ thin films with thicknesses of 360 Å were annealed at temperatures varied from 70 to 130 °C. The thicknesses of the five blends from 1:3 to 1:6 SQ:$PC_{70}BM$ cast from 20 mg/mL solutions in chloroform, as determined by using Woolam VASE ellipsometer, were 1660, 1530, 720, 730, and 760 Å. The absorption spectra of the pure and blended films on quartz substrates with various compositions were measured using a Perkin-Elmer Lambda 1500 UV-NIR spectrometer.

The ionization potential energy for the SQ thin film was measured by ultraviolet photoemission spectroscopy (UPS) using 21.22 eV He−I emission in a Thermo VG Scientific Clam4MCD analyzer system. Samples were prepared by thermal evaporation onto a p-type Si substrate of a 30 nm thick Au film, followed by a 10 nm thick SQ film. Transfers between the deposition chambers and the analysis chamber were performed at $<10^{-8}$ Torr, while the UPS pressure was $<10^{-9}$ Torr. The analyzer resolution was ~0.15 eV as determined by a fit to the Fermi level of Au.

Samples for atomic force microscopy (AFM) operated in the tapping mode were prepared by first casting SQ:$PC_{70}BM$ blend thin films on ITO-coated glass substrates with an 80 Å thick molybdenum oxide (MoO_3) film predeposited on its surface by thermal evaporation. The films were annealed at 70 °C for 10 min in a N_2 glovebox.

The active layers of the PV cells consisted of SQ in $PC_{70}BM$ blends prepared from totally dissolved solids in chloroform in air. The weight ratios of SQ to $PC_{70}BM$ were varied as in the case of the XRD samples. The separate solutions of SQ and $PC_{70}BM$ were first stirred at room temperature for 12 h before the solutions were mixed to form the blends, which were then stirred for 2 h and used to spin-coat the active layers at rates ranging from 1000 rpm to 6000 rpm for 30 s.

Devices were fabricated as follows: The ITO-coated glass substrate was precleaned with organic solvents and exposed to ultraviolet/ozone following procedures described elsewhere.[10,15] Measurements of thin film hole mobility used the following sandwich structures: ITO/poly(3,4-ethylenedioxythiphene) poly(styrenesulfonate) (PEDOT:PSS) (460 Å)/SQ(360 Å)/Au (1000 Å) and ITO/PEDOT:PSS(460 Å)/SQ:$PC_{70}BM$/Au (1000 Å). Solar cells employed the following structure: ITO/MoO_3(80 Å)/SQ:$PC_{70}BM$(*x* Å)/Al(1000 Å). Here, MoO_3 is thermally evaporated onto the ITO surface in a vacuum system with a base pressure of 10^{-7} Torr. Solutions containing a mixture of SQ:$PC_{70}BM$ (3:1 and 1:1) with a concentration of 10 mg/mL, and SQ:$PC_{70}BM$ (1:2, 1:3, and 1:6) with 20 mg/mL in chloroform were cast on the MoO_3. The films with thicknesses of 320, 400, 720, 730, and 760 Å were then annealed at 70 °C for 10 min in an ultrahigh purity N_2 ambient. The devices were completed by thermally evaporating a 1000 Å thick Al cathode through a shadow mask resulting in a device area of 7.9×10^{-3} cm^2. For comparison, we also fabricated a 1:6 SQ:$PC_{60}BM$ cell with the same structure as the analogous SQ:$PC_{70}BM$ device.

Using similar procedures, control SQ/C_{60} and SQ/C_{70} planar cells were fabricated with the following structure: ITO/MoO_3(80 Å)/SQ(62 Å)/fullerene(400 Å)/bathocuproine (BCP)(100 Å)/Al(1000 Å). The SQ thin film in this case was spin-coated from 1 mg/mL SQ solution in dichloromethane at a rate of 3000 rpm for 30 s, followed by annealing at 110 °C for 10 min.

The current density−voltage (*J*−*V*) characteristics and η_p of the devices were measured using an Oriel 150 W solar simulator irradiation from a Xe arc lamp with AM1.5G filters and an NREL-calibrated standard Si detector. Measurements and solar spectral correction were made using standard methods.[29] The EQE was measured using monochromated light from a Xe-lamp, chopped at 400 Hz, and focused to the device active area.

Acknowledgment. We thank Ning Li, Jeramy Zimmerman, Brian Lassiter, Kuen-Ting Shiu, Gregory McGraw, Kai Sun, and Richard R. Lunt III for helpful discussions and suggestions. This work was supported in part by the Air Force Office of Scientific Research (G.W.), the Department of Energy, Office of Basic Energy Sciences as part of Energy Frontier Research Centers: The Center for Solar and Thermal Energy Conversion at the University of Michigan (award DE-SC0000957, S.R.F.) and the Center for Energy Nanoscience at the University of Southern California (award DE-SC0001011, S.W. and M.E.T.), and Global Photonic Energy Corporation (K.R.).

REFERENCES AND NOTES

1. Janssen, R. A. J.; Hummelen, J. C.; Sariciftci, N. S. Polymer−Fullerene Bulk Heterojunction Solar Cells. *MRS Bull.* **2005**, *30*, 33–36.
2. Duren, J. K. J.; Yang, X. N.; Loos, J.; Bulle-Lieuwma, C. W. T.; Sieval, A. B.; Hummelen, J. C.; Janssen, R. A. Relating the Morphology of Poly(-phenylene vinylene)/Methanofullerene Blends to Solar-Cell Performance. *Adv. Funct. Mater.* **2004**, *14*, 425–434.
3. Mühlbacher, D.; Scharber, M.; Morana, M.; Zhu, Z. G.; Waller, D.; Gaudiana, R.; Brabec, C. High Photovoltaic Performance of a Low-Bandgap Polymer. *Adv. Mater.* **2006**, *18*, 2884–2889.
4. Li, G.; Shrotriya, V.; Huang, J.; Yao, Y.; Moriarty, T.; Emery, K.; Yang, Y. High-Efficiency Solution Processable Polymer Photovoltaic Cells by Self-Organization of Polymer Blends. *Nat. Mater.* **2005**, *4*, 864–868.
5. Park, S. H.; Roy, A.; Beaupré, S.; Cho, S.; Coates, N.; Moon, J. S.; Moses, D.; Leclerc, M.; Lee, K.; Heeger, A. J. Bulk Heterojunction Solar Cells with Internal Quantum Efficiency Approaching 100%. *Nat. Photonics* **2009**, *3*, 297–302.
6. Lenes, M.; Kooistra, F. B.; Hummelen, J. C.; Severen, I. V.; Lutsen, L.; Vanderzande, D.; Cleij, T. J.; Blom, P. W. M.

Charge Dissociation in Polymer:Fullerene Bulk Heterojunction Solar Cells with Enhanced Permittivity. *J. Appl. Phys.* **2008**, *104*, 114517.
7. Moulé, A. J.; Meerholz, K. Morphology Control in Solution-Processed Bulk-Heterojunction Solar Cell Mixtures. *Adv. Funct.Mater.* **2009**, *19*, 3028–3036.
8. Lioyd, M. T.; Anthony, J. E.; Malliaras, G. G. Photovoltaics from Soluble Small Molecules. *Mater. Today* **2007**, *10*, 34–41.
9. Peumans, P.; Uchida, S.; Forrest, S. R. Efficient Bulk Heterojunction Photovoltaic Cells Using Small-Molecular-Weight Organic Thin Films. *Nature* **2003**, *425*, 158–162.
10. Yang, F.; Sun, K.; Forrest, S. R. Efficient Solar Cells Using All-Organic Nanocrystalline Networks. *Adv. Mater.* **2007**, *19*, 4166.
11. Silverstri, F.; Irwin, M. D.; Beverina, L.; Facchetti, A.; Pagani, G. A.; Marks, T. J. Efficient Squaraine-Based Solution Processable Bulk-Heterojunction Solar Cells. *J. Am. Chem. Soc.* **2008**, *130*, 17640–17641.
12. Tamayo, A. B.; Dang, X. D.; Walker, B.; Seo, J. W.; Kent, T.; Nguyen, T. Q. A Low Band Gap, Solution Processable Oligothiophene with a Dialkylated Diketopyrrolopyrrole Chromophore for Use in Bulk Heterojuntion Solar Cells. *Appl. Phys. Lett.* **2009**, *94*, 103301.
13. Walker, B.; Tamayo, A. B.; Dang, X. D.; Zalar, P.; Seo, J. H.; Garcia, A.; Tantiwiwat, M.; Nguyen, T. Q. Nanoscale Phase Separation and High Photovoltaic Efficiency in Solution-Processed, Small-Molecule Bulk Heterojunction Solar Cells. *Adv. Funct. Mater.* **2009**, *19*, 3063–3069.
14. Wang, S. Y.; Mayo, E. I.; Perez, M. D.; Griffe, L.; Wei, G. D.; Djurovich, P. I.; Forrest, S. R.; Thompson, M. E. High Efficiency Organic Photovoltaic Cells Based on a Vapor Deposited Squaraine Donor. *Appl. Phys. Lett.* **2009**, *94*, 233304.
15. Rand, B. P.; Xue, J. G.; Uchida, S.; Forrest, S. R. Mixed Donor−acceptor Molecular Heterojunctions for Photovoltaic Applications. I. Material Properties. *J. Appl. Phys.* **2005**, *98*, 124902.
16. Tian, M. Q; Furuki, M.; Iwasa, I.; Sato, Y.; Pu, L. S.; Tatsuura, S. Search for Squaraine Derivatives That Can Be Sublimed without Thermal Decomposition. *J. Phys. Chem. B* **2002**, *106*, 4370.
17. Boultif, A.; Louër, D. Powder Pattern Indexing with the Dichotomy Method. *J. Appl. Crystallogr.* **2004**, *37*, 724–731.
18. Ashwell, G. J.; Bahra, G. S.; Brown, C. R.; Hamilton, D. G.; Kennard, C. H. L.; Lynch, D. E. 2,4-Bis[4-(*N*,*N*-dibutylamino) phenyl] Squaraine: X-ray Crystal Structure of a Centrosymmetric Dye and the Second-Order Nonlinear Optical Properties of Its Noncentrosymmetric Langmuir−Blodgett Films. *J. Mater. Chem.* **1996**, *6*, 23–26.
19. Lamper, M. A.; Mark, P. Academic: New York, 1970.
20. Li, N.; Lassiter, B. E.; Lunt, R. R.; Wei, G. D.; Forrest, S. R. Open Circuit Voltage Enhancement Due to Reduced Dark Current in Small Molecule Photovoltaic Cells. *Appl. Phys. Lett.* **2009**, *94*, 023307.
21. Lunt, R. R.; Giebink, N. C.; Belak, A. A.; Benziger, J. B.; Forrest, S. R. Exciton Diffusion Lengths of Organic Semiconductor Thin Films Measured by Spectrally Resolved Photoluminescence Quenching. *J. Appl. Phys.* **2009**, *105*, 053711.
22. Schilinsky, P.; Waldauf, C.; Hauch, J.; Brabec, C. J. Simulation of Light Intensity Dependent Current Characteristics of Polymer Solar Cells. *J. Appl. Phys.* **2004**, *95*, 023307.
23. Rand, B. P.; Burk, D. P.; Forrest, S. R. Offset Energies at Organic Semiconductor Heterojunctions and Their Influence on the Open-Circuit Voltage of Thin-Film Solar Cells. *Phys. Rev. B* **2007**, *75*, 115327.
24. Giebink, N. C.; Lassiter, B. E.; Forrest, S. R. MRS 2009 Fall Meeting, Boston, MA, 2009.
25. Perez, M. D.; Borek, C.; Forrest, S. R.; Thompson, M. E. Molecular and Morphological Influences on the Open Circuit Voltages of Organic Photovoltaic Devices. *J. Am. Chem. Soc.* **2009**, 9281–9286.
26. Peumans, P.; Forrest, S. R. Separation of Geminate Charge-Pairs at Donor−Acceptor Interfaces in Disordered Solids. *Chem. Phys. Lett.* **2004**, *398*, 27–31.
27. Koster, L. J. A.; Smits, E. C. P.; Mihailetchi, V. D.; Blom, P. W. M. *Phys. Rev. B* **2005**, *72*, 085205.
28. Lenes, M.; Morana, M.; Brabec, C. J.; Blom, P. W. M. Recombination-Limited Photocurrents in Low Bandgap Polymer/Fullerene Solar Cells. *Adv. Funct. Mater.* **2009**, *19*, 1106.
29. Shrotriya, V.; Li, G.; Yao, Y.; Morarty, T.; Emery, K.; Yang, Y. Accurate Measurement and Characterization of Organic Solar Cells. *Adv. Funct. Mater.* **2006**, *16*, 2016–2023.